



# Spatiotemporal variations in ecological quality of Otindag Sandy Land based on a new modified remote sensing ecological index

ZHAO Xiaohan<sup>1</sup>, HAN Dianchen<sup>1</sup>, LU Qi<sup>2</sup>, LI Yunpeng<sup>3</sup>, ZHANG Fangmin<sup>1\*</sup>

<sup>1</sup> Collaborative Innovation Center on Forecast and Evaluation of Meteorological Disasters/Jiangsu Key Laboratory of Agricultural Meteorology, Nanjing University of Information Science and Technology, Nanjing 210044, China;

<sup>2</sup> Institute of Desertification, Chinese Academy of Forestry, Beijing 100091, China;

<sup>3</sup> Ecology and Agricultural Meteorology Center of Inner Mongolia Autonomous Region, Hohhot 010051, China

**Abstract:** Otindag Sandy Land in China is an important ecological barrier to Beijing; the changes in its ecological quality are major concerns for sustainable development and planning of this area. Based on principal component analysis and path analysis, we first generated a modified remote sensing ecological index (MRSEI) coupled with satellite and ground observational data during 2001–2020 that integrated four local indicators (greenness, wetness, and heatness that reflect vegetation status, water, and heat conditions, respectively, as well as soil erosion). Then, we assessed the ecological quality in Otindag Sandy Land during 2001–2020 based on the MRSEI at different time scales (i.e., the whole year, growing season, and non-growing season). MRSEI generally increased with an upward rate of 0.006/a during 2001–2020, with clear seasonal and spatial variations. Ecological quality was significantly improved in most regions of Otindag Sandy Land but degraded in the southern part. Regions with ecological degradation expanded to 18.64% of the total area in the non-growing season. The area with the worst grade of MRSEI shrunk by 15.83% of the total area from 2001 to 2020, while the area with the best grade of MRSEI increased by 9.77% of the total area. The temporal heterogeneity of ecological conditions indicated that the improvement process of ecological quality in the growing season may be interrupted or deteriorated in the following non-growing season. The implementation of ecological restoration measures in Otindag Sandy Land should not ignore the seasonal characteristics and spatial heterogeneity of local ecological quality. The results can explore the effectiveness of ecological restoration and provide scientific guides on sustainable development measures for drylands.

**Keywords:** ecological quality; modified remote sensing ecological index; principal component analysis; path analysis; Otindag Sandy Land; dryland ecosystem

**Citation:** ZHAO Xiaohan, HAN Dianchen, LU Qi, LI Yunpeng, ZHANG Fangmin. 2023. Spatiotemporal variations in ecological quality of Otindag Sandy Land based on a new modified remote sensing ecological index. *Journal of Arid Land*, 15(8): 920–939. <https://doi.org/10.1007/s40333-023-0065-9>

## 1 Introduction

Otindag Sandy Land in China presents a crucial ecological barrier and is a typical and fragile dryland ecosystem adjacent to Beijing (the capital of China) that is suffering from structural damage to parafunction, leading to land degradation and biodiversity loss (Wang et al., 2017; Wu et al., 2019). To slow down the process of land degradation and improve the ecological

\*Corresponding author: ZHANG Fangmin (E-mail: Fmin.zhang@nuist.edu.cn)

Received 2023-01-28; revised 2023-05-30; accepted 2023-06-03

© Xinjiang Institute of Ecology and Geography, Chinese Academy of Sciences, Science Press and Springer-Verlag GmbH Germany, part of Springer Nature 2023

environment, China has implemented a series of ecological restoration projects, such as the Three-North Shelter Forest Program and the Beijing-Tianjin sand source control project (Wu et al., 2013; Sun et al., 2019; Wen et al., 2020). Nevertheless, there is a continued debate on the effectiveness of these ecological restoration projects that have been implemented for 20 years (Yuan et al., 2016; Ma et al., 2017; Sun et al., 2019; Cong et al., 2022). A quantitative assessment of spatiotemporal dynamics in ecological quality is essential for the sustainable development of Otindag Sandy Land.

With the rapid development of remote sensing and GIS technology, several remote sensing-based indices had been proposed to present the characteristics of ecological quality (Xu, 2013; Xu et al., 2018; Wei et al., 2020). For instance, Wei et al. (2020) calculated the environmental vulnerability distance index by considering hydro-meteorological, socio-economic, soil-biological, and topographical factors to assess the ecological quality of Shiyang River Basin in China. Xu et al. (2018) developed a remote sensing ecological index (RSEI) based on the principal component analysis (PCA) to avoid the artificial influences on weights and yield more objective and reasonable; thus, this index has been widely used in the regional ecological quality assessment. However, researchers also realized that RSEI might have problems in ecological quality assessment in areas where urbanization may not be the main factor influencing ecological quality (Wang et al., 2020; Zhu et al., 2021; Yao et al., 2022; Ye and Kuang, 2022; Zhao et al., 2022). Therefore, the traditional RSEI has been improved and expanded in recent years. For example, Wang et al. (2020) developed an arid remote sensing ecological index (ARSEI) by replacing the dryness indicator in RSEI with the indicators of salinity and land degradation. Yao et al. (2022) modified RSEI with bare soil index and salinity index to reflect the macro ecological quality in arid areas. For applications in rocky desertified areas, Ye and Kuang (2022) constructed a modified remote sensing ecological index (MRSEI) by combining the degree of rocky desertification. An improved composite remote sensing ecological index (CRSEI) was developed by incorporating population density for studying the ecological quality of Yellow River Delta, China (Zhao et al., 2022). In addition, to adapt to the local contradictions, researchers have developed new RSEI that can accurately characterize the changes in regional ecological quality, such as the remote sensing ecological index of local adaptation improvement (RSEILA) (Zhu et al., 2021).

Ecological quality reflects the comprehensive characteristics of the elements, structures and functions of an ecosystem (Wu et al., 2019). Dryland is a special ecosystem type with sparse precipitation and high evaporation (Wu et al., 2019). In dryland ecosystem, vegetation is an important guarantee of regional ecosystem stability and greening is a major measure to mitigate desertification (Mamat et al., 2018; Chen et al., 2022). Meanwhile, water and heat are the principal natural conditions for vegetation growth and ecosystem development (Wang et al., 2021). Dryland ecosystem is the most fragile ecosystem, which is extremely vulnerable to human activities and climate change (Chen et al., 2022; Cong et al., 2022). Thus, soil erosion is a major reason for soil degradation and desertification in drylands that may augment when soil erosion proceeds faster than pedogenesis (IPCC, 2019). Soil erosion also reduces the capacity of water and soil conservation, affects regional water reserves, and threatens ecological quality seriously (Masroor et al., 2022). In this study, with a focus on comprehensive ecological quality assessment based on the regional characteristics of drylands, we combined the vegetation status, water and heat conditions, and soil erosion into an integrated index to assess the ecological quality in Otindag Sandy Land.

As aforementioned, remote sensing image processing technology is flourishing; ecological indices based on remote sensing technology have been increasingly used in ecological quality assessment. However, adverse atmospheric states, sensor failures, and revisit periods still inevitably restrict the continuity of remote sensing data and hinder the wide application of remote sensing-based ecological indices (Qureshi et al., 2020; Yang et al., 2022a). Multiple data reconstruction methods aiming at improving the image quality, such as the maximum value composite, local filtering, and function fitting (Priyadarshi et al., 2018; Yang et al., 2022a, b; Zheng et al., 2022), are sound candidates, albeit these methods are highly dependent on the reliability of remote sensing data. Therefore, based on the PCA and path analysis of four

representative indicators (greenness, wetness, heatness, and soil erosion) of ecological quality in Otindag Sandy Land, this study attempted to construct a modified RSEI (i.e., MRSEI) coupled with satellite and ground observational data. Specifically, a long-time series MRSEI data (2001–2020) at different time scales (i.e., the whole year, growing season, and non-growing season) were calculated and used to assess ecological quality and its spatiotemporal variations in Otindag Sandy Land. The results can explore the effectiveness of ecological restoration and provide scientific guides on sustainable development measures in Otindag Sandy Land as well as other similar dryland regions in the world.

## 2 Materials and methods

### 2.1 Study area

Otindag Sandy Land (41°46′–45°69′N, 111°55′–118°38′E) is located in the central part of Inner Mongolia Autonomous Region, China, and is one of the major sandy areas in the world (John et al., 2009; Ma et al., 2017). The landform of this area is relatively undulating, with a roughly higher terrain in the southeast and a lower terrain in the northwest, covering an area of approximately  $0.17 \times 10^6 \text{ km}^2$  (Liu and Wang, 2010). Otindag Sandy Land belongs to the arid and semi-arid continental climate zone, with the annual average temperature of  $0.9^\circ\text{C}$ – $5.5^\circ\text{C}$ . Affected by the monsoon, precipitation is gradually becoming less from the southeast to the northwest, with annual precipitation decreasing from 350–400 mm to 100–200 mm (Lou et al., 2019). Grassland is the major land cover type distributed across the area, accounting for 81.37% of the total area in 2020. Forests are patchy (5.13%) in the east while croplands are found in the south and east, occupying 1.92% of the total area (Fig. 1a). From 2001 to 2020, the land cover transformation occurred in 17.97% of the total area, of which 11.35% was transformed from grassland to cropland, 27.03% from bare land to grassland, and 11.18% from cropland to grassland, while 6.18% represented afforestation (Fig. 1b).

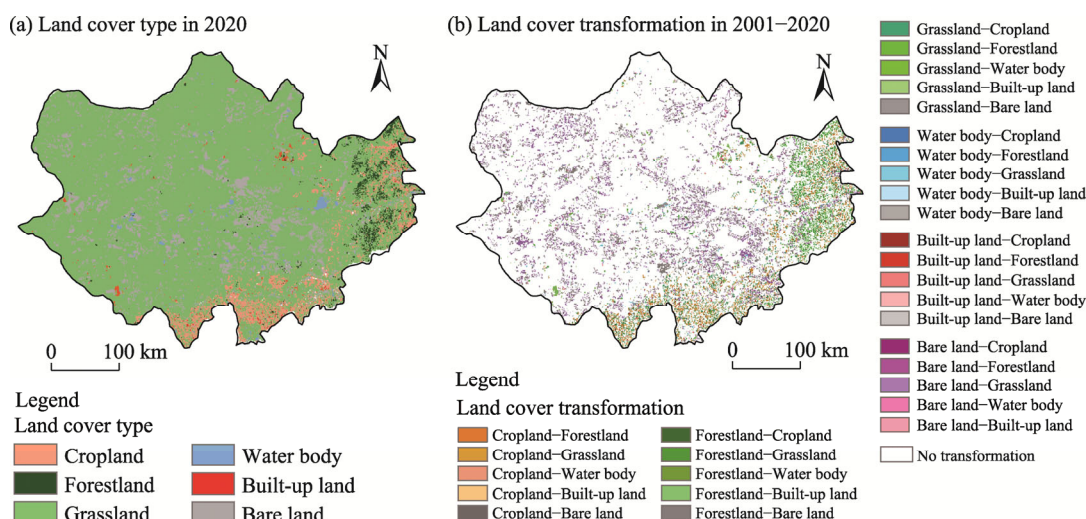


**Fig. 1** Spatial distribution of different land cover types in Otindag Sandy Land in 2020 (a) and land cover transformation from 2001 to 2020 (b). The 1-km gridded land use cover datasets in 2000 and 2020 were derived from the Resource and Environment Science and Data Center (<http://www.resdc.cn>).

### 2.2 Data sources and processing

Monthly Normalized Difference Vegetation Index (NDVI) products (MOD13A3) from the Moderate-resolution Imaging Spectroradiometer (MODIS) at a spatial resolution of 1 km (from January 2001 to December 2020) were collected from the National Aeronautics and Space Administration (NASA) (<https://ladsweb.modaps.eosdis.nasa.gov>). NDVI data were used to

calculate greenness index ( $I_g$ ).

The daily meteorological data (2001–2020) of 103 weather stations, including the average air temperature (°C), maximum air temperature (°C), minimum air temperature (°C), relative humidity (%), sunshine duration (h), wind speed (m/s), and precipitation (mm) were from the National Meteorological Science Data Center (<http://data.cma.cn>). These data have undergone quality control (e.g., outlier rejection) to ensure their authenticity and reasonableness. We interpolated the daily data after quality control based on the Australian National University Spline (ANUSPLIN) software (Hutchinson and Xu, 2013), and extracted the final 1-km spatial meteorological datasets of Otindag Sandy Land for calculating wetness index ( $I_w$ ), heatness index ( $I_h$ ), and soil erosion index ( $I_s$ ). ANUSPLIN has the advantages of solid theory of thin plate spline function and high interpolation accuracy by the incorporation of parametric linear sub-model, in addition to the independent spline variables; this software has been widely used in meteorological variables (Fick and Hijmans, 2017; Guo et al., 2020).

Soil dataset, including soil types, soil organic matter content, soil sand and clay contents, and the percentage of soil organic carbon (SOC), was obtained from the China Soil Characteristics Dataset of the National Cryosphere Desert Data Center (<http://www.ncdc.ac.cn>) that was calculated from the 1:1,000,000 soil database of the second national soil census in China. The 30-m digital elevation model (DEM) data were downloaded from the Geospatial Data Cloud (<http://www.gscloud.cn>). Soil dataset and DEM were used to calculate  $I_s$ .

All above datasets were projected to the UTM-WGS84 coordinate system and resampled to 1 km spatial resolution by the nearest neighbor resampling. Moreover, datasets for the whole year and in the growing season were calculated by the monthly average data of January through December and May through September, respectively; while for the non-growing season, datasets were calculated by the monthly average data of October through April of the next year.

The 1-km gridded land use cover datasets in 2000 and 2020 were derived from the Resource and Environment Science and Data Center (<http://www.resdc.cn>). There were six categories of land cover types in this study: cropland, forestland, grassland, water body, bare land, and built-up land (John et al., 2009).

### 2.3 Construction of modified remote sensing ecological index (MRSEI)

Considering the regional characteristics of the dryland ecosystem in Otindag Sandy Land, we selected the vegetation status, water and heat conditions, and soil erosion to represent the local indicators of ecological quality in Otindag Sandy Land. The four indicators include  $I_g$ ,  $I_w$ ,  $I_h$ , and  $I_s$ . Figure 2 shows the flowchart of spatiotemporal analysis of ecology quality in Otindag Sandy Land with MRSEI in this study.

Vegetation cover is not only an important environmental element but also an indicator of the sensitive state of terrestrial ecosystems, and plays an important role in the analysis and evaluation of regional ecological and environmental factors (Tian and Min, 1998; Xu et al., 2019).  $I_g$  reflects the growth status and distribution characteristics of green vegetation in the study area, and is expressed by Equation 1.

$$I_g = (\text{NDVI} - \text{NDVI}_{\text{soil}}) / (\text{NDVI}_{\text{veg}} - \text{NDVI}_{\text{soil}}), \quad (1)$$

where  $\text{NDVI}_{\text{soil}}$  and  $\text{NDVI}_{\text{veg}}$  are the NDVI values for the areas covered with bare soil and complete vegetation, respectively.

$I_w$  is expressed by the ratio of regional total precipitation to total potential evapotranspiration, which can effectively characterize the regional wet and dry conditions to determine the water requirements of ecosystems (Fernandes et al., 2016). It was calculated by the following equation:

$$I_w = \text{PRE} / \text{ET}_0, \quad (2)$$

where, PRE is the total precipitation (mm); and  $\text{ET}_0$  is the total potential evapotranspiration (mm), which was calculated based on the Penman-Monteith model using the interpolated climate datasets (Allen et al., 1998; Chen, 2021).

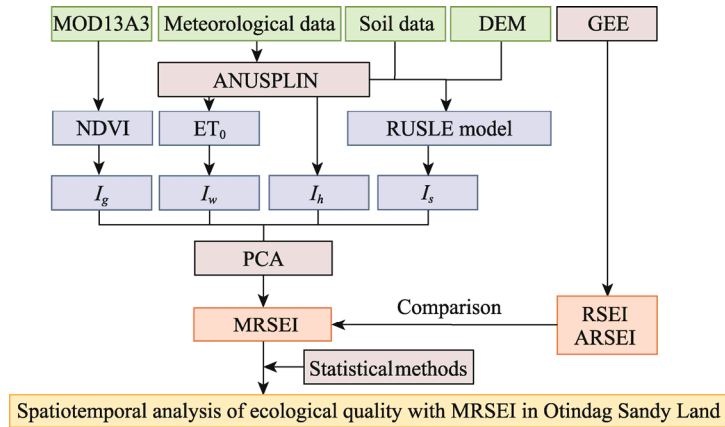


**Fig. 2** Flowchart for constructing modified remote sensing ecological index (MRSEI) and spatiotemporal analysis of ecology quality with MRSEI in Otindag Sandy Land. MOD13A3, Monthly Normalized Difference Vegetation Index (NDVI) products from the Moderate-resolution Imaging Spectroradiometer (MODIS); DEM, digital elevation model; GEE, Google Earth Engine; ANUSPLIN, Australian National University Spline; NDVI, Normalized Difference Vegetation Index; ET<sub>0</sub>, total potential evapotranspiration;  $I_g$ , greenness index;  $I_w$ , wetness index;  $I_h$ , heatness index;  $I_s$ , soil erosion index; PCA, principal component analysis; RSEI, remote sensing ecological index; ARSEI, arid remote sensing ecological index.

$I_h$  is closely related to the energy exchange processes within the ecosystem and reveals the potential amount of vegetation cover, which is expressed by the land surface temperature, an important indicator of the surface environment (Coutts et al., 2016). In this study, we replaced the land surface temperature in RSEI derived from remote sensing data (Xu et al., 2018) by air temperature from the National Meteorological Science Data Center (<http://data.cma.cn>).

$I_s$  was calculated by the Revised Universal Soil Loss Equation (RUSLE) model, which synthetically considers the effects of precipitation and runoff on near-surface soil; this model has been widely used for the assessment of water and soil erosion (Toy and Osterkamp, 1995; Masroor et al., 2022). The indicator  $I_s$  was calculated as follows:

$$I_s = A_p - A_r, \quad (3)$$

$$A_p = R \times K \times L \times S, \quad (4)$$

$$A_r = R \times K \times L \times S \times C \times P, \quad (5)$$

$$R = \sum_{k=1}^{24} \left( \left( \sum_{i=1}^n \sum_{j=0}^N \alpha \times P a_{i,j,k}^{1.7265} \right) / n \right), \quad (6)$$

$$K = (-0.1383 + 0.51575 K_{\text{EPIC}}) \times 0.1317, \quad (7)$$

$$K_{\text{EPIC}} = \left( 0.2 + 0.3 e^{-0.0256 m_s (1 - m_{\text{silt}}/100)} \right) \times \left[ m_{\text{silt}} / (m_c + m_{\text{silt}}) \right]^{0.3} \\ \times \left[ 1 - 0.25 \text{SOC} / (\text{SOC} + e^{3.72 - 2.95 \text{SOC}}) \right] \\ \times \left[ 1 - 0.7 (1 - m_s/100) + e^{-5.51 + 22.9 (1 - m_s/100)} \right], \quad (8)$$

$$L = (\lambda / 22.13)^m, \quad (9)$$

$$m = \begin{cases} 0.02 & \theta < 0.5^\circ \\ 0.03 & 0.5^\circ < \theta < 1.5^\circ \\ 0.04 & 1.5^\circ < \theta < 3.0^\circ \\ 0.05 & \theta \geq 3.0^\circ \end{cases}, \quad (10)$$

$$S = \begin{cases} 10.8 \sin \theta + 0.03 & \theta < 5^\circ \\ 16.8 \sin \theta + 0.05 & 5^\circ < \theta < 10^\circ \\ 21.9 \sin \theta - 0.96 & \theta \geq 10^\circ \end{cases} \quad (11)$$

where,  $A_P$  and  $A_r$  are the potential and actual soil erosion ( $\text{t}/(\text{km}^2 \cdot \text{a})$ ), respectively;  $R$  is the factor of precipitation erosion ( $\text{MJ} \cdot \text{mm}/(\text{km}^2 \cdot \text{h} \cdot \text{a})$ );  $K$  is the factor of soil erodibility ( $\text{t} \cdot \text{h}/(\text{MJ} \cdot \text{mm})$ );  $L$  and  $S$  are the factors of the length and angle of the slope, respectively (dimensionless);  $C$  is the factor of vegetation cover and management; and  $P$  is the factor of soil and water conservation measures.  $Pa_{i,j,k}$  represents the  $j^{\text{th}}$  daily precipitation with erosiveness on the  $k^{\text{th}}$  half a month of the  $i^{\text{th}}$  year, where  $k$  is the serial number of half a month in a year ( $k=1, 2, \dots, 24$ ) and  $i$  is the serial number of years ( $i=1, 2, \dots, n$ ). The  $j$  and  $N$  are the serial number and cumulative frequency of daily precipitation with erosiveness on the  $k^{\text{th}}$  half a month of the  $i^{\text{th}}$  year, respectively.  $K_{\text{EPIC}}$  is the factor of soil erodibility in pre-revision.  $m_c$ ,  $m_{\text{silt}}$ , and  $m_s$  represent the percentage contents of clay ( $<0.002$  mm), silt ( $0.002$ – $0.050$  mm), sand ( $0.050$ – $2.000$  mm), respectively, with the unit of %. SOC is the percentage of soil organic carbon (%).  $\lambda$  is the horizontal slope length (m),  $m$  is the slope length index, and  $\theta$  is the slope degree ( $^\circ$ ). The elaborate calculation method of model factors refers to the study of Masroor et al. (2022).

The above four indicators ( $I_g$ ,  $I_w$ ,  $I_h$ , and  $I_s$ ) were projected to the UTM-WGS84 coordinate system at the spatial resolution of 1 km and temporal resolution of 1 month during 2001–2020, and then normalized to the dimensionless form in the range of 0–1.

The weight for initial MRSEI (denoted as  $\text{MRSEI}_0$ ) based on the aforementioned four normalized indicators from 2001 to 2020 was calculated through PCA. This approach effectively avoids the bias of results caused by different artificial defined weights, making the results more objective and reliable (Hang et al., 2020). During 2001–2020, the contribution rates of the first component (PC1) were all greater than 73.00%, indicating that PC1 had integrated most of the characteristics of the four indicators (Fig. 3); therefore, PC1 was chosen to calculate the  $\text{MRSEI}_0$ . The formula of  $\text{MRSEI}_0$  is expressed as follows:

$$\text{MRSEI}_0 = 1 - [\text{PC1}(I_g, I_w, I_h, I_s)], \quad (12)$$

where,  $\text{MRSEI}_0$  is the initial value of MRSEI (from  $-1.000$  to  $1.000$ ) at different time scales (i.e., the whole year, growing season, and non-growing season) for the given year.

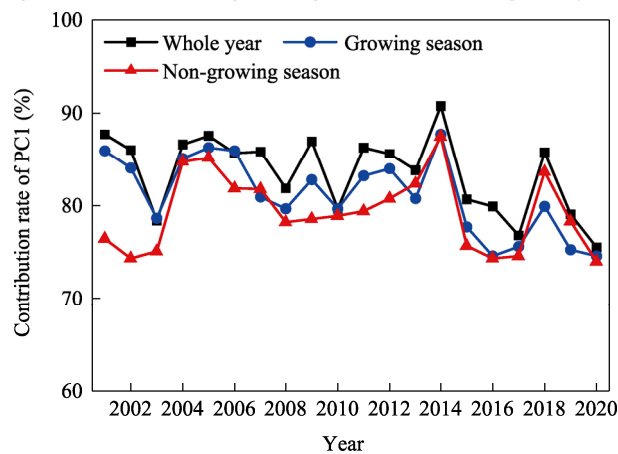


**Fig. 3** Contribution rates of the first principal component (PC1) of MRSEI indicators (greenness, wetness, heatness, and soil erosion) at the whole year, growing season, and non-growing season scales from 2001 through 2020

To facilitate the comparison among different time periods, we normalized the  $\text{MRSEI}_0$  values to obtain the final MRSEI value based on Equation 13.

$$\text{MRSEI} = (\text{MRSEI}_0 - \text{MRSEI}_{0\min}) / (\text{MRSEI}_{0\max} - \text{MRSEI}_{0\min}), \quad (13)$$

where  $MRSEI_{0max}$  and  $MRSEI_{0min}$  are the maximum and minimum values of  $MRSEI_0$ , respectively. The higher  $MRSEI$  values indicate better ecological quality, while the lower  $MRSEI$  values represent poorer ecological quality. According to the Technical Criterion for Ecosystem Status Evaluation issued by the Ministry of Environmental Protection of China (Wang et al., 2021), we divided  $MRSEI$  (0.000–1.000) into five grades (worst: 0.000–0.200; poor: 0.200–0.400; general: 0.400–0.600; good: 0.600–0.800; and best: 0.800–1.000) for further analysis.

## 2.4 Statistical analysis

### 2.4.1 Path analysis

Path analysis is widely used to explore causal structure patterns between dependent and independent variables based on factor analysis and multiple linear regression (Fan et al., 2016; Shao et al., 2022). In this study, we regarded  $MRSEI$  as the dependent variable and  $I_g$ ,  $I_w$ ,  $I_h$ , and  $I_s$  as the independent variables to clarify the correlations between them and initially verify the reliability and effectiveness of  $MRSEI$ . The larger the absolute value of path coefficient, the stronger the effect of the independent variable on  $MRSEI$ . The plus or minus path coefficient means its promotion or inhibition of  $MRSEI$ , respectively.

### 2.4.2 Trend analysis

Theil-Sen's slope method is a very useful nonparametric method for estimating linear trend (John et al., 2013; Xu et al., 2019). Therefore, it was used in this study to calculate the slope of each variable in each pixel and analyze the distribution pattern of the change trend (John et al., 2013). The slope ( $\beta$ ) represents the change rate of variables. If the slope is negative ( $\beta < 0$ ), it indicates that the variable is decreasing; otherwise, the variable is increasing ( $\beta > 0$ ). In addition, the non-parametric Mann-Kendall test (Niu et al., 2023) was used to evaluate the significance of the change trend of variables. The trend of  $MRSEI$  in Otindag Sandy Land was categorized into four types: significant increase ( $\beta > 0$  and  $P < 0.05$ ), increase ( $\beta > 0$  and  $P > 0.05$ ), significant decrease ( $\beta < 0$  and  $P < 0.05$ ), and decrease ( $\beta < 0$  and  $P > 0.05$ ).

### 2.4.3 Barycenter model

Because the dynamic variation of the barycenter can reflect the contrast and shift of regional element distribution (Huang et al., 2021), it was used to perform spatial analysis of barycenter changes in this study. The barycenter of  $MRSEI$  was calculated using the following equations:

$$X = \sum_{i=1}^I x_i \times CRR_i / \left( \sum_{i=1}^I CRR_i \right), \quad (14)$$

$$Y = \sum_{j=1}^J y_j \times CRR_j / \left( \sum_{j=1}^J CRR_j \right), \quad (15)$$

where,  $X$  and  $Y$  are the coordinates of latitude and longitude of the barycenter, respectively;  $x_i$  and  $y_i$  are the coordinates of latitude and longitude corresponding to the  $i^{\text{th}}$  and  $j^{\text{th}}$  pixels, respectively;  $I$  and  $J$  are the number of pixels of latitude and longitude, respectively;  $CRR_i$  and  $CRR_j$  are the  $MRSEI$  values corresponding to the  $i^{\text{th}}$  and  $j^{\text{th}}$  pixels, respectively.

All data processing and analysis were executed in Python 3.7 (Anaconda Inc., Austin, USA), and the visualization implementation was conducted in OriginPro 2023 (OriginLab Inc., Northampton, USA) and ArcMap 10.2 (Esri Inc., Redlands, USA).

## 2.5 Validation

To further assess the feasibility of  $MRSEI$ , we compared  $MRSEI$  with the traditional  $RSEI$  (Xu, 2013) and  $ARSEI$  for arid areas (Wang et al., 2020) based on 1-km MODIS datasets.  $RSEI$  was constructed with four indicators, including greenness, wetness, dryness, and heatness, whereas  $ARSEI$  took five indicators into account, comprising greenness, wetness, heatness, salinity, and land degradation. In this study, we calculated  $RSEI$  and  $ARSEI$  in the growing season of 2001, 2005, 2010, 2015, and 2020 based on PCA via the Google Earth Engine. More information about the principles of  $RSEI$  and  $ARSEI$  can be found in Xu (2013) and Wang et al. (2020), respectively.

### 3 Results

#### 3.1 Feasibility analysis of MRSEI

The four indicators ( $I_g$ ,  $I_w$ ,  $I_h$ , and  $I_s$ ) of MRSEI were calculated by PCA on the basis of their contribution rates. Because the PC1 of the four indicators from 2001 to 2020 can integrate the most of the indicator characteristics, we took 2001 and 2020 as typical years with more detailed analysis. The subsequent path analysis further verified the significant correlation between the four indicators and MRSEI.

As shown in Table 1, the PC1 loads of  $I_g$ ,  $I_w$ , and  $I_s$  were positive, and the average PC1 load of  $I_w$  (0.63) was larger than those of  $I_s$  (0.06) and  $I_g$  (0.35). This indicated that all these three indicators had positive effects on MRSEI, and the contribution rate of  $I_w$  was higher than those of  $I_s$  and  $I_g$ , which was consistent with the results from path analysis. Furthermore, it was confirmed with the actual situation that precipitation is the key environmental factor in this area. Conversely, the PC1 loads of  $I_h$  were negative, and the absolute value of its average load (0.68) was greater than those of  $I_g$ ,  $I_w$ , and  $I_s$ . This indicated that  $I_h$  had a negative effect on MRSEI, and its contribution to MRSEI was higher than  $I_g$ ,  $I_w$ , and  $I_s$ , also consisting with the results from path analysis. In addition, the absolute value of the PC1 load for  $I_h$  was the highest in 2001, but the absolute value of the PC1 load for  $I_w$  was the highest in 2020, indicating that the main influencing indicator of MRSEI changed from  $I_h$  in 2001 to  $I_w$  in 2020. The values of PC1 loads for the whole year were roughly close to those in the growing season, implying that ecological quality was affected more in the whole year than in the growing season. Therefore, it can be concluded that MRSEI based on PC1 is feasible and can be used to conduct the ecological quality assessment of Otindag Sandy Land.

As shown in Figure 4 based on path analysis,  $I_w$  was the most important indicator affecting MRSEI with a highly significant correlation between them in all time periods from 2001 to 2020, followed by  $I_g$ ,  $I_h$ , and  $I_s$  in sequence.  $I_h$  and MRSEI were negatively correlated, and the correlation was strong in the non-growing season.  $I_g$  was positively and significantly correlated with MRSEI, with correlation coefficients of 0.80 in the growing season and 0.66 in the non-growing season, indicating that the influence of vegetation status (greenness) was weakened in the non-growing season. The results of path analysis also verified the feasibility of MRSEI from another perspective.

**Table 1** PC1 of MRSEI indicators ( $I_g$ ,  $I_w$ ,  $I_h$ , and  $I_s$ ) in 2001 and 2020

Year	Time scale	PC1 load				Eigenvalue	Accumulated contribution rate (%)
		$I_g$	$I_w$	$I_h$	$I_s$		
2001	Whole year	0.32	0.54	−0.78	0.04	0.14	87.72
	Growing season	0.40	0.57	−0.72	0.06	0.11	84.10
	Non-growing season	0.31	0.47	−0.82	0.06	0.06	74.46
2020	Whole year	0.37	0.73	−0.57	0.06	0.08	73.95
	Growing season	0.44	0.73	−0.52	0.06	0.08	74.53
	Non-growing season	0.24	0.72	−0.65	0.06	0.06	73.96

Note: PC1, first principal component of principal component analysis; MRSEI, modified remote sensing ecological index;  $I_g$ , greenness index;  $I_w$ , wetness index;  $I_h$ , heatness index;  $I_s$ , soil erosion index.

#### 3.2 Spatial changes of ecological quality

The average MRSEI values in Otindag Sandy Land from 2001 to 2020 at different time scales are shown in Figures 5 and 6. The regions with the worst and poor grades of MRSEI at the whole year scale were scattered in the west of Otindag Sandy Land (Fig. 5a1), accounting for 10.55% and 17.29% of the total area on average, respectively. As shown in Figure 5b1 and c1, the regions with these grades (worst and poor) shrunk in the growing season (8.92% and 15.96% of the total area, respectively) but expanded to the eastside of Otindag Sandy Land in the non-growing



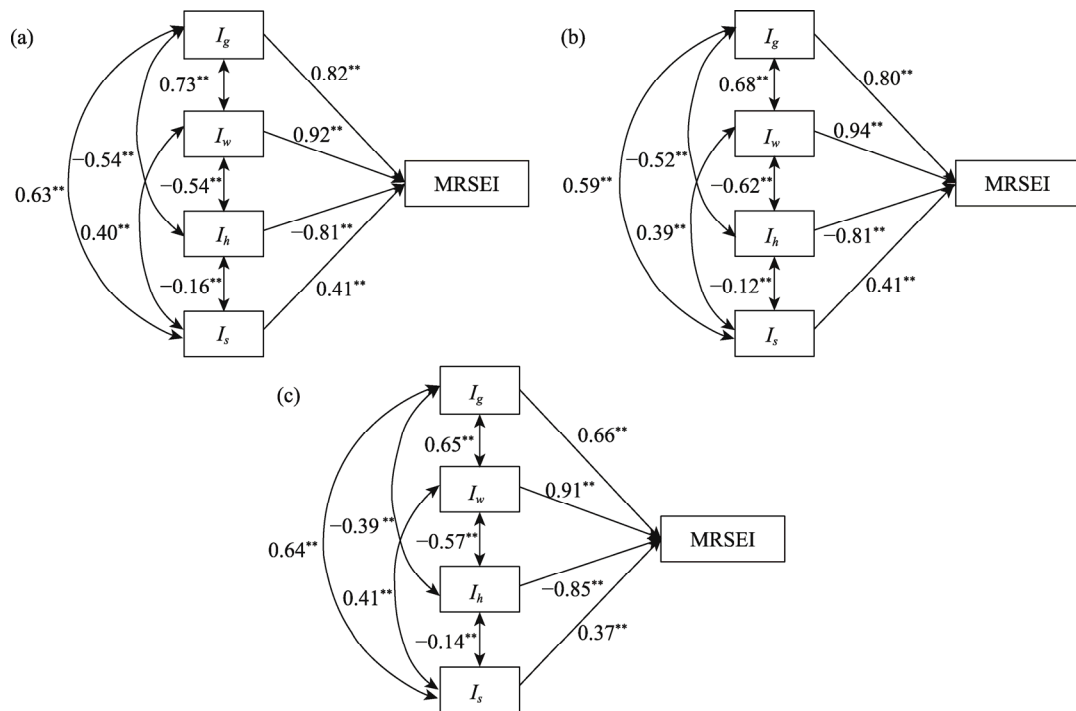


**Fig. 4** Path analysis of MRSEI and its four indicators ( $I_g$ ,  $I_w$ ,  $I_h$ , and  $I_s$ ) in Otindag Sandy Land at the whole year (a), growing season (b), and non-growing season (c) scales from 2001 through 2020. Value around the double arrows indicates the correlation coefficient between independent variables, while value around the single arrow represents the path coefficient between independent and dependent variables. \*, passing the 0.05 significant test; \*\*, passing the 0.01 significant test.

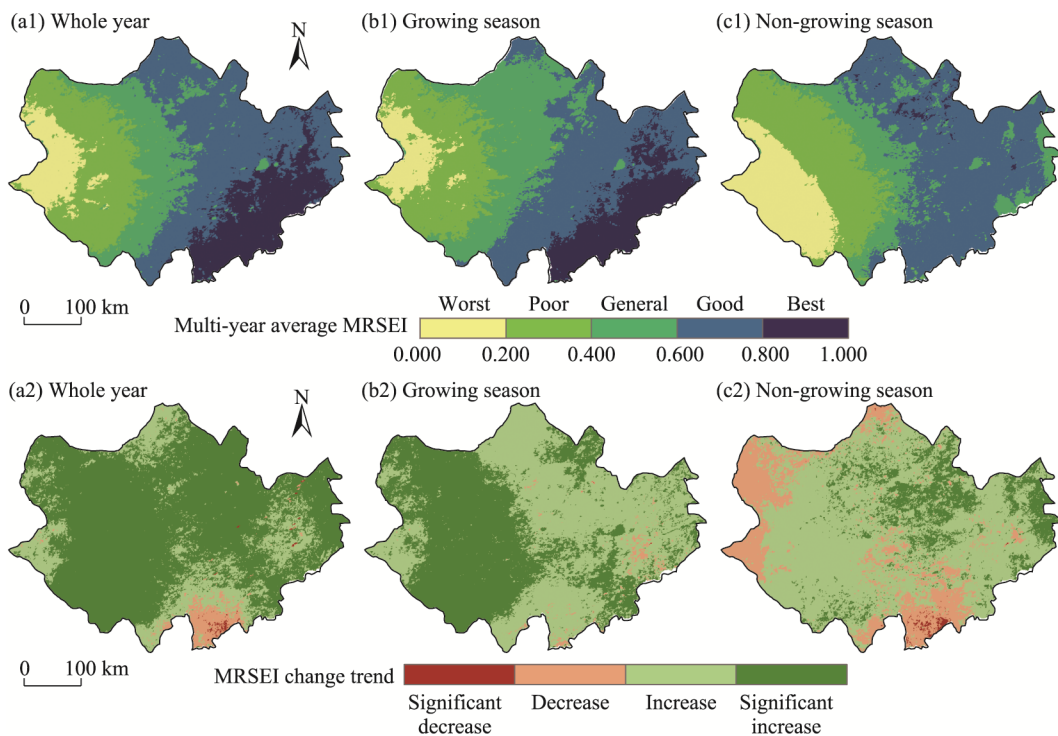


**Fig. 5** Spatial distributions of multi-year average MRSEI and the corresponding MRSEI change trend at the whole year (a1 and a2), growing season (b1 and b2), and non-growing season (c1 and c2) scales from 2001 to 2020

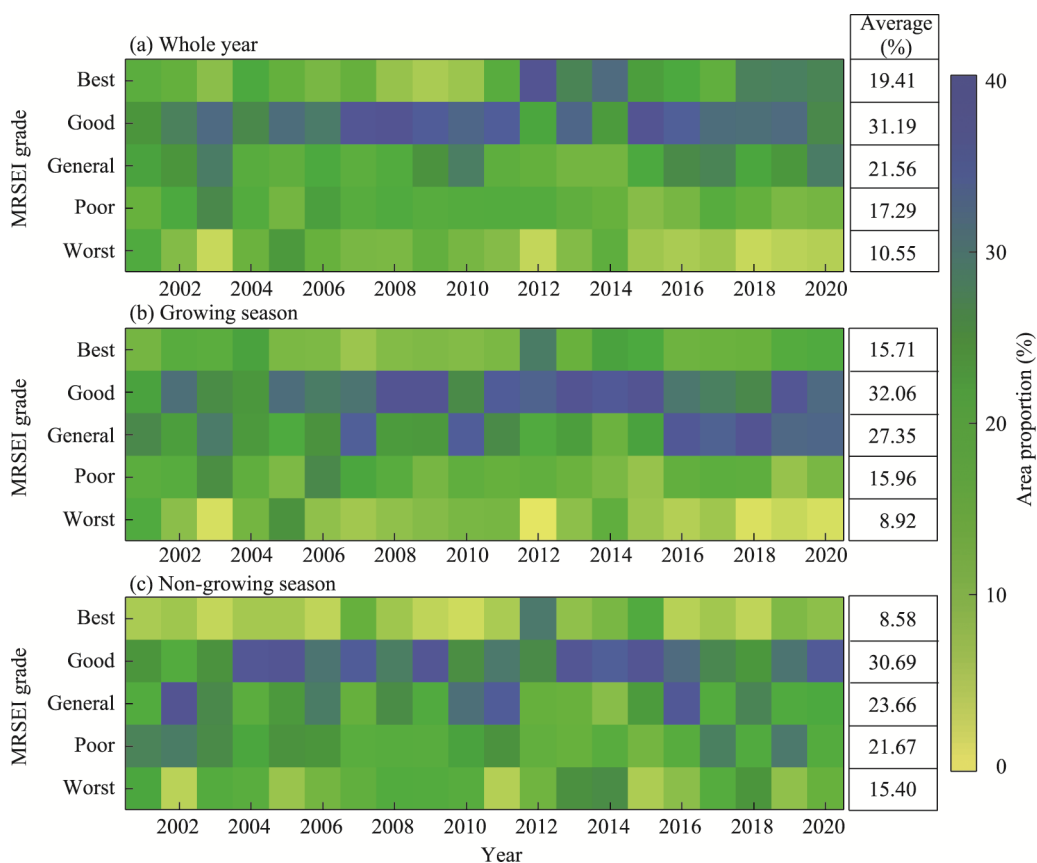


**Fig. 6** Area proportions of different MRSEI grades in Otindag Sandy Land at the whole year (a), growing season (b), and non-growing season (c) scales from 2001 to 2020

season (15.40% and 21.67% of the total area, respectively). In addition, the increased areas with the worst grade of MRSEI in the non-growing season expanded to most regions in Sonid Right Banner (Fig. 5c1). On the other hand, the regions with the good and best grades of MRSEI were mostly found in the southeastern part of Otindag Sandy Land, which accounted for 31.19% and 19.41% of the total area, respectively (Fig. 5b1), but the regions with the best grade of MRSEI were transformed to the good and general grades in the non-growing season (Fig. 5c1). This resulted in the regions with the best grade of MRSEI decreasing to 8.58% of the total area in the non-growing season.

Correspondingly, the variations of MRSEI across Otindag Sandy Land varied considerably in space over the past 20 years. MRSEI at the whole year scale increased in 96.56% of the total area, with 75.62% of the total area showing a significant increasing trend ( $P < 0.05$ ; Fig. 5a2). The increase of MRSEI in the western and southern parts of Otindag Sandy Land mainly existed in the growing season (Fig. 5b2), while the increase of MRSEI in the northern part and eastside of Otindag Sandy Land mostly existed in the non-growing season (Fig. 5c2). In contrast, MRSEI at the whole year scale decreased in the remaining regions (3.44% of the total area), mostly distributed in Taibus Banner of the southern part of Otindag Sandy Land, mainly due to its ecological degradation in the non-growing season. In addition, the regions with the decreased MRSEI reached 18.64% of the total area in the non-growing season, which were scattered in the southern, western, and northern parts of Otindag Sandy Land; however, only 0.27% of the total area showed significant decrease in MRSEI ( $P < 0.05$ ). The comparison of MRSEI in 2001, 2005, 2010, 2015, and 2020 further indicated that ecological quality in the growing season was stably improved in the whole Otindag Sandy Land, while MRSEI in the non-growing season showed a

stronger inter-annual fluctuation (Fig. S1). Severe ecological quality degradation was found in the non-growing season of 2010, which was mainly occurred in the southern and northern parts of Otindag Sandy Land (Fig. S1). Overall, it appeared that ecological quality over most regions of Otindag Sandy Land had improved from 2001 to 2020, but there were still some small patches showed degradation in ecological quality.

Table 2 exhibits the area transfer matrix of MRSEI grades at the whole year scale from 2001 to 2020. Relative to 2001, the area with the best, good, and general grades of MRSEI increased while the area with the worst and poor grades of MRSEI decreased in 2020. The area with the best and good grades of MRSEI increased by 20,493.89 km<sup>2</sup> (from 30,214.83 km<sup>2</sup> in 2001 to 47,105.73 km<sup>2</sup> in 2020 for the best grade and from 42,136.76 km<sup>2</sup> in 2001 to 45,739.75 km<sup>2</sup> in 2020 for the good grade, accounting for 9.77% and 2.09% of the total area, respectively), with most converted from the area with the general grade of MRSEI (19,351.89 km<sup>2</sup>), and 1142.00 km<sup>2</sup> from the area with the worse and poor grades of MRSEI. Meanwhile, the area degrading from the good grade of MRSEI to the general grade was 2254.99 km<sup>2</sup>. The area with the general grade of MRSEI in 2020 increased by 10,668.94 km<sup>2</sup>, accounting for 6.17% of the total area. The area with the worst grade of MRSEI was significantly decreased by 27,357.84 km<sup>2</sup> (from 35,832.79 km<sup>2</sup> in 2001 to 8474.95 km<sup>2</sup> in 2020), indicating that only 4.90% of Otindag Sandy Land had the worst grade of MRSEI in 2020.

**Table 2** Area transfer matrix of MRSEI with different grades in Otindag Sandy Land from 2001 to 2020 (unit: km<sup>2</sup>)

	Worst	Poor	General	Good	Best	Total (2001)
Worst	8462.95	18,262.89	8648.95	458.00	0.00	35,832.79
Poor	12.00	3571.98	21,380.88	684.00	0.00	25,648.86
General	0.00	9.00	17,351.23	21,541.88	65.00	38,967.11
Good	0.00	0.00	2254.99	22,205.87	17,675.90	42,136.76
Best	0.00	0.00	0.00	850.00	29,364.83	30,214.83
Total (2020)	8474.95	21,843.87	49,636.05	45,739.75	47,105.73	172,800.35

### 3.3 Temporal evolution of ecological quality

Figure 7a shows the temporal variations in the ecological quality of Otindag Sandy Land from 2001 to 2020. MRSEI in the growing season exhibited a significant increasing trend with the change rate of 0.004/a ( $P < 0.05$ ) from 2001 to 2020. The corresponding trend in the non-growing season slowed down after 2010 with insignificant change rate ( $P > 0.05$ ). In addition, the inter-annual fluctuation was high in the non-growing season, such as the dramatic decline from 2015 to 2018. Due to the dominance of MRSEI in the growing season, the change of MRSEI at the whole year scale followed the change trend of MRSEI in the growing season; specifically, it increased significantly with the change rate of 0.006/a ( $P < 0.05$ ) from 2001 to 2020.

Figure 7b–d depicts the barycenter movements of MRSEI from 2001 to 2020. The longitudinal barycenter of MRSEI at the whole year scale declined ( $P < 0.05$ ) and tended to move by 0.2° toward the west. However, the latitudinal barycenter was barely unchanged and did not pass the significant test ( $P > 0.05$ ). It can be seen that the longitudinal and latitudinal barycenter changes of MRSEI at the whole year scale were basically determined by the shifts in the growing season. The longitudinal and latitudinal barycenter of MRSEI in the non-growing season showed an insignificant increasing trend ( $P > 0.05$ ), with the longitudinal barycenter inclining back to the east and the latitudinal barycenter at a higher latitude. The longitudinal movement direction of the barycenter in the non-growing season was opposite to that in the growing season in some years (e.g., 2005 and 2015). On the whole, the barycenter of MRSEI in Otindag Sandy Land tended to move westward, which indicated that in the past 20 years, ecological quality in the western part of Otindag Sandy Land has improved significantly.

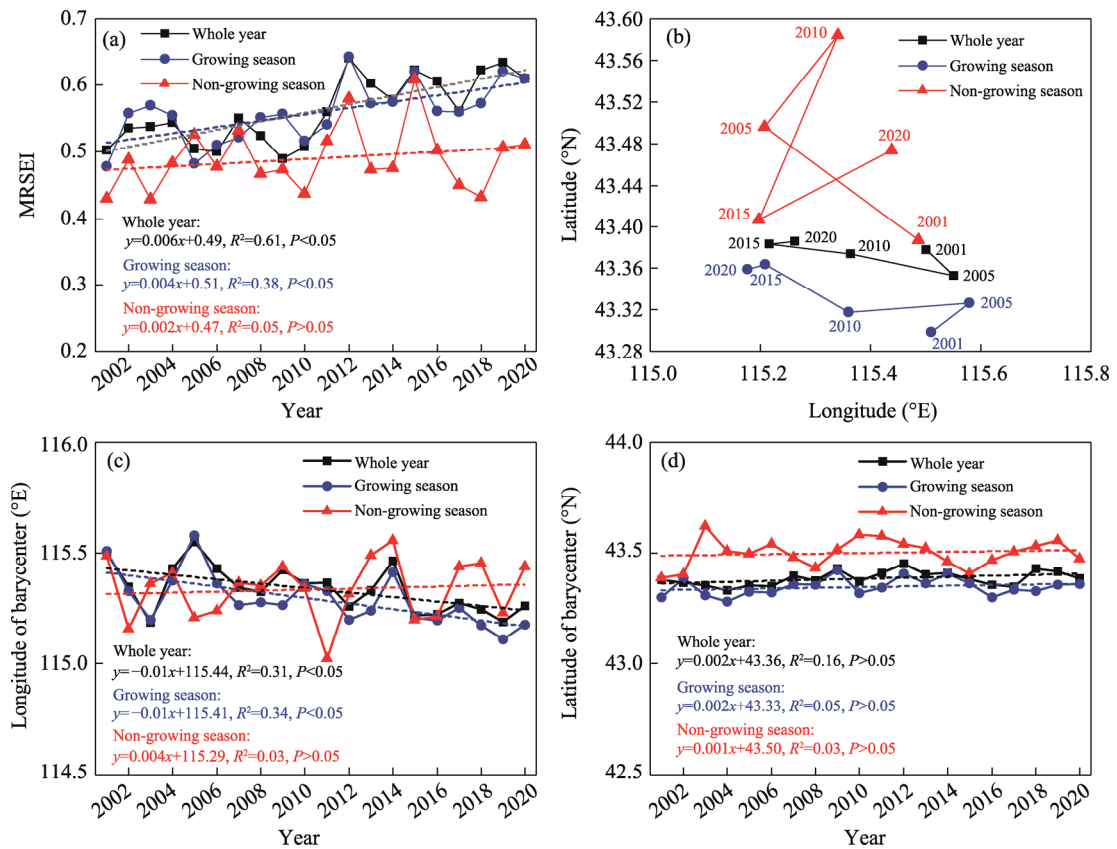


**Fig. 7** Temporal change of MRSEI in Otindag Sandy Land (a) and its barycenter movements (b–d) at the whole year, growing season, and non-growing season scales from 2001 to 2020

### 3.4 Impact of climate and land cover on ecological quality

Figure 8a1 and a2 depicts the relationships of MRSEI changes with the variations in precipitation and air temperature. Precipitation was positively related to MRSEI; specifically, precipitation showed an increment of 1.5 mm/a, corresponding to an increase of MRSEI by 0.002 ( $\pm 0.002$ ) per year (Fig. 8a1). In contrast, air temperature was negatively related to MRSEI (Fig. 8b1); specifically, air temperature decreased by 0.02°C/a, corresponding to an increase of MRSEI by 0.002 ( $\pm 0.003$ ) per year. However, precipitation and air temperature were not linearly related to the changes in MRSEI. The degree of MRSEI changes became more apparent when the increase of precipitation was higher than 4.5 mm/a and the decrease of air temperature was more than 0.02°C/a. As seen from Figure 8a2, precipitation showed increasing trends over the whole Otindag Sandy Land, with the change rates of 1.5–4.5 mm/a in more than 76.49% of the total area, whereas the increment of precipitation of more than 4.5 mm/a was only found in the middle of Sonid Right Banner and Sonid Left Banner in the western part of Otindag Sandy Land. Correspondingly, air temperature decreased in the same regions where the increment of precipitation was more than 4.5 mm/a (Fig. 8b2). This synergistic effect directly increased MRSEI, which significantly improved ecological quality from the worst grade to poor or general grade (Figs. 5 and S1).

Land cover types had different effects on MRSEI. For the four major land cover types in Otindag Sandy Land (forestland, cropland, grassland, and bare land), the multi-year average MRSEI was 0.805, 0.779, 0.544, and 0.433, respectively (Fig. 8c1). For land cover changes (Fig. 8c2), MRSEI increased by 0.004 ( $\pm 0.004$ ) per year for both the conversion of cropland to grassland and the inversion of grassland to cropland. The transformation of bare land to grassland increased MRSEI by 0.006 ( $\pm 0.004$ ) per year. Afforestation was the most effective forcing to improve MRSEI in the study area, with MRSEI increased by 0.009 ( $\pm 0.004$ ) per year.

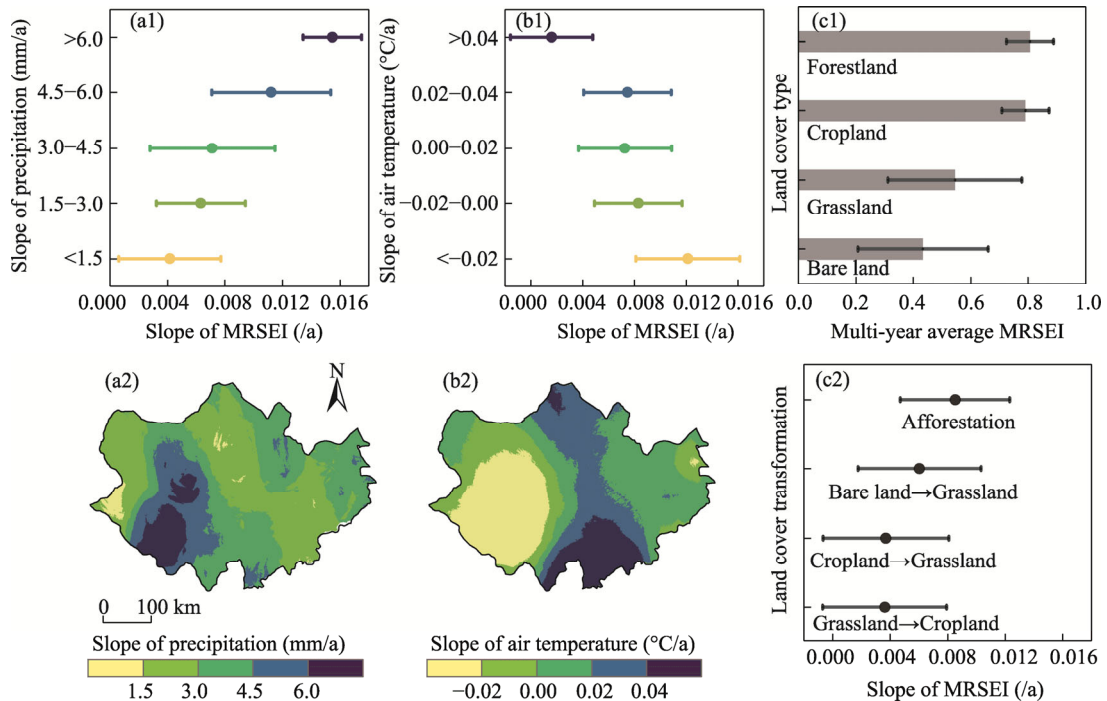


**Fig. 8** Relationships of the slope of MRSEI with the slopes of precipitation (a1) and air temperature (b1), and spatial distributions of changes in precipitation (a2) and air temperature (b2), as well as multi-year average MRSEI over different land cover types (c1) and MRSEI changes with transformation of land cover types (c2). Bars mean standard errors; dot means the average of the slope of MRSEI. Colors in Figure 8a1 and b1 correspond to color classes in Figure 8a2 and b2, respectively.

## 4 Discussion

### 4.1 Validation of the effectiveness of MRSEI

We examined the ability of MRSEI to capture the local texture information of water bodies and topography (Fig. 9). Figure 9a showed that MRSEI could accurately capture the shape of Dalai Nur Lake and the presence of some small lakes, as well as the higher vegetation coverage in the east of Otindag Sandy Land, where MRSEI values were also higher. Meanwhile, MRSEI accurately captured the annular vegetation coverage zone with the change of topography, as well as the buildings in the southeastern part of annular zone that corresponded to lower MRSEI values (Fig. 9b). Clearly, MRSEI could well reflect the actual scene of land surface in Otindag Sandy Land.

Comparisons among the contribution rates of PC1 of RSEI, MRSEI, and ARSEI indicators in the growing seasons of 2001, 2005, 2010, 2015, and 2020 are shown in Figure 10a. The contribution rates of PC1 of MRSEI indicators were the highest in all years, followed by RSEI and ARSEI indicators. Furthermore, the spatiotemporal variations were compared among these three indices (Fig. 10b). RSEI, ARSEI, and MRSEI depicted similar low-high zonal changes, with values increasing from the west to the east and culminating at nearly 117°–118°E, but they showed different spatial heterogeneity, with MRSEI being the highest and RSEI being the lowest. Interestingly, all these three indices exhibited increasing trends at the temporal scales, but their change rates were slightly different. Overall, all these three indices reflected that ecological quality was improved in Otindag Sandy Land over the past 20 years. However, RSEI did not consider the local characteristics of Otindag Sandy Land (e.g., soil erosion) in drylands even though the contribution rates of PC1 of RSEI indicators were higher than 70.00%. The contribution rates of PC1 of ARSEI indicators were between 56.50%–68.38%. In this case, if only the PC1 was considered, much information may be omitted (Jiang et al., 2021). Therefore,

MRSEI can be considered as an effective alternative index for ecological quality assessment in Otindag Sandy Land. Our results also showed that the selection of indicators should ideally be adapted to the local contradictions so that it can accurately characterize the changes in regional ecological quality.

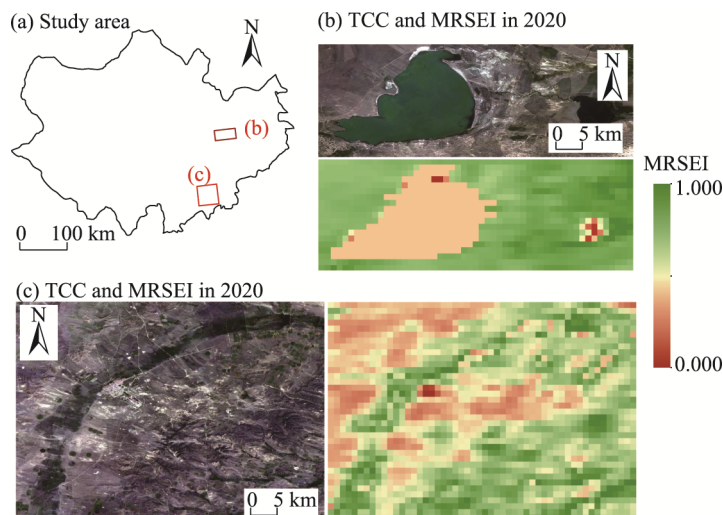


**Fig. 9** Local validation of MRSEI in capturing the texture information of water bodies (a and b) and topography (a and c) between MRSEI and real scenes of surface in 2020. TCC is the true color composite image (RGB 432) of Landsat 8 filtered; it was calculated by the median composite method of the images with the cloud cover of less than 5% in the growing season (from May to September) in 2020 by the Google Earth Engine.

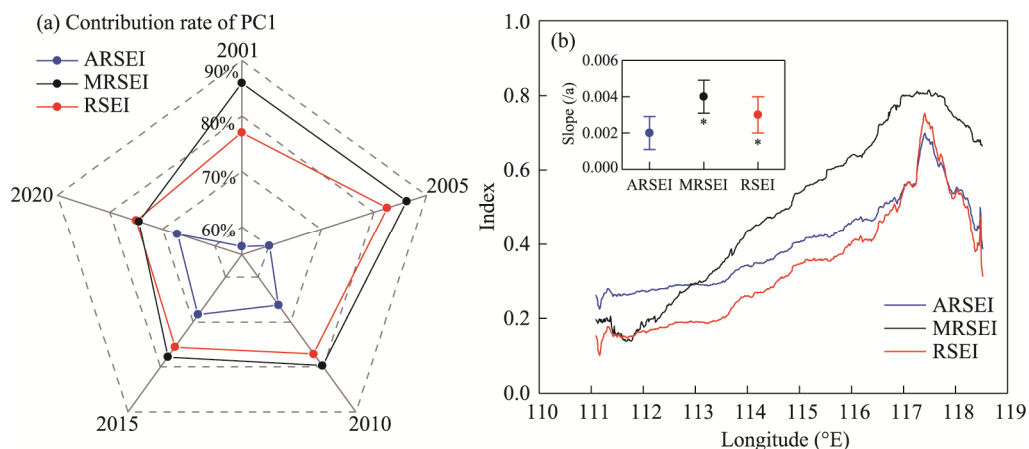


**Fig. 10** Comparison between the contribution rates of PC1 of RSEI, MRSEI, and ARSEI indicators in the growing seasons of 2001, 2005, 2010, 2015, and 2020 (a) and zonal distribution and temporal changes (the inset) of RSEI, MRSEI, and ARSEI (b). \*, passing the 0.05 significant test. Bars mean standard errors and dot means the average of slope.

## 4.2 Impact of climate and land cover on MRSEI

Based on the results of PCA and path analysis, the wetness indicator played a major role in improving ecological quality, which confirmed the pivotal status of water resources in arid and semi-arid areas (Wu et al., 2022). In Otindag Sandy Land, precipitation in the eastern and northeastern parts is higher (Ma et al., 2017), which is consistent with the spatial distribution of MRSEI. The western part of Otindag Sandy Land with less precipitation and sparser vegetation (Shi et al., 2004) was rated as the region with the worst grade of MRSEI. The fragile ecosystems in Otindag Sandy Land are sensitive to water resources, and spatial differences in water resources



can lead to the heterogeneity of ecological quality in Otindag Sandy Land.

The overall ecological quality in Otindag Sandy Land was improved from 2001 to 2020, but it showed large inter-annual variations. The improved regions accounted for approximately 96.56% of the total area across Otindag Sandy Land. The main reason is that climate in Otindag Sandy Land becomes more humid (Xu et al., 2020; Zhao et al., 2021), as shown in Figure 8, which is conducive to relieving local water resources shortage. Increased precipitation tends to improve vegetation coverage, especially in the western part of Otindag Sandy Land with grasslands and bare lands (Cong et al., 2022), where MRSEI increased significantly and ecological quality was improved (Fig. 5). However, the reported warming in the non-growing season might cause the evapotranspiration increased and soil dried out (Zhang et al., 2019; Xu et al., 2020). The improvement process of vegetation and soil conditions in the growing season were interrupted or deteriorated in the following non-growing season (Fig. 5). These results indicated that ecological quality has seasonal changes, and attention should be paid to its seasonal degradation. Given that future climate will get more humid in this region, there is still room for sustainable ecological improvement in Otindag Sandy Land from the water supply perspective.

In addition to the influence of climate change, the implementation of ecological restoration measures in Otindag Sandy Land, such as maintaining grass and livestock balance, returning farmland to forests, and implementing enclosures and grazing prohibitions (Yuan et al., 2016; Ma et al., 2017), can be conducive to improving the ecological quality of Otindag Sandy Land. Due to the effectiveness of these measures, regional vegetation has been effectively restored, which alleviated ecological deterioration to some extent, especially for the grasslands and bare lands. Combined with the increase in precipitation, many regions with poorer ecological quality (worst and poor grades) were transformed into regions with better ecological quality (general, good, and best grades). Afforestation in the forest regions of the eastern part of Otindag Sandy Land with richer precipitation directly increased NDVI, in turn, enhanced ecological quality therein. However, afforestation may lower the groundwater level in arid areas (Chen et al., 2018; Lu et al., 2018). We therefore recommend that local climate change and water resources should be taken fully into account when implementing ecological restoration measures.

In terms of land cover and land use change, grassland is the dominant land cover type in Otindag Sandy Land; the quality of grasslands has been improved over the last 20 years due to increased precipitation and ecological restoration measure implementations. The land cover type with denser vegetation had higher MRSEI. However, this does not mean that the changes of higher MRSEI in the regions with denser vegetation are positive. For example, higher MRSEI in the southern part of Otindag Sandy Land decreased, especially in the non-growing season. As shown in Figure 1, the transformation of grasslands to croplands as well as the expansion of croplands that occurred in the southern part of Otindag Sandy Land may lead to soil salinization and degradation of natural habitats (Tang et al., 2021; Zhuang et al., 2021), which can explain the degradation in the southern part of Otindag Sandy Land with good ecological quality, especially in Taibus Banner. In sum, ecological restoration is important for sustainable development, but local economic benefits from agriculture and husbandry expansion must not be ignored. Thus, how to balance local economic benefits and ecological revitalization is the most crucial factor for regional ecological sustainability in the future.

Although the MRSEI changes in Otindag Sandy Land showed that ecological quality is gradually improving, there are still uncertainties in restoring ecological quality in the future. According to previous studies (e.g., Chen et al., 2020), these highly precipitation-sensitive regions are ecologically fragile and easily suffer from droughts because of rain-fed vegetation properties, so both the significant inter-annual and seasonal fluctuations of precipitation and the increased water consumption due to rapid warming can increase the threat of short-term drought to its local ecosystems (John et al., 2013). Thus, the seasonal evaluation of ecological conditions as well as corresponding conservations are very important. How to reasonably and scientifically formulate measures to improve the ecological quality of Otindag according to local characteristics and environmental conditions needs further evaluations. From this study, the priority is to

maintain the natural landscapes and avoid overgrazing in the western part of Otindag Sandy Land with scarce water resources. In regions with severe ecological degradation, it is essential to implement graded governance and encourage local tourism to satisfy the harmonious development of economy and nature. On the other hand, since the development of MRSEI aims to explore the ecological quality of Otindag Sandy Land with typical dryland ecosystem, its practicality is temporarily limited to dryland ecosystems, and whether it is appropriate to extend to a broader area needs further research.

## 5 Conclusions

In this study, we constructed the MRSEI integrating greenness, wetness, heatness, and soil erosion indicators coupled with the local characteristics and environmental conditions based on PCA and path analysis to evaluate the ecological quality of Otindag Sandy Land from 2001 to 2020. All contribution rates of PC1 were above 73.00% during 2001–2020. MRSEI based on PC1 appeared promising in Otindag Sandy Land. Results of PCA and path analysis showed that greenness, wetness, and soil erosion indicators had positive effects on MRSEI, whereas heatness had a negative effect. The contribution rate of PC1 of wetness was the highest, followed by heatness, greenness, and soil erosion.

In the past 20 years (2001–2020), the changes of ecological quality in Otindag Sandy Land showed seasonal and regional differences. Ecological quality in the growing season was improved significantly, but in the non-growing season it fluctuated with an insignificant increasing trend. Spatially, the regions with the good and best grades of MRSEI were mostly distributed in the eastern part of Otindag Sandy Land, while the regions with the worst and poor grades of MRSEI were concentrated in the western part of Otindag Sandy Land. However, the regions with the worst and poor grades of MRSEI respectively accounted for 8.92% and 15.96% of the total area in the growing season but 15.40% and 21.67% of the total area in the non-growing season. Ecological equality was improved in most regions of Otindag Sandy Land in the growing season but degraded in the western, northern and southern parts of Otindag Sandy Land in the non-growing season (18.64% of the total area). Altogether, the area with the worst grade of MRSEI shrunk by 15.83% of the total area during the study period, from 35,832.79 km<sup>2</sup> in 2001 to 8474.95 km<sup>2</sup> in 2020, while the area with the best grade of MRSEI in the east increased by 9.77% of the total area from 30,214.83 km<sup>2</sup> in 2001 to 47,105.73 km<sup>2</sup> in 2020. Over time, spatiotemporal variations of ecological equality varied with seasons. Such seasonal differences should be taken into account for better reflecting ecological quality assessment results. For multi-year analysis, we suggest to choose indicators to represent seasonal ecological conditions according to the local characteristics of the study area.

## Conflict of interest

The authors declare that they have no known competing financial interests or personal relationships that could have appeared to influence the work reported in this paper.

## Acknowledgments

We acknowledge the financial support given by the Special Funds for Science and Technology Innovation on Carbon Peak Carbon Neutral of Jiangsu Province, China (BK20220017), the Innovation Development Project of China Meteorological Administration (CXFZ2023J073), and the National Key R&D Program of China (2018YFC1506606).

## Author contributions

Conceptualization: ZHAO Xiaohan, HAN Dianchen, ZHANG Fangmin; Methodology: ZHAO Xiaohan, HAN Dianchen; Formal analysis: ZHAO Xiaohan, HAN Dianchen; Writing - original draft preparation: ZHAO Xiaohan, HAN Dianchen, ZHANG Fangmin; Writing - review and editing: ZHAO Xiaohan, ZHANG Fangmin;



Funding acquisition: LU Qi, LI Yunpeng, ZHANG Fangmin; Resources: LI Yunpeng, ZHANG Fangmin; Supervision: LU Qi, ZHANG Fangmin.

## References

- Allen R G, Pereira L S, Raes D, et al. 1998. Crop evapotranspiration: Guidelines for computing crop requirements. In: FAO Irrigation and Drainage Paper 56. Rome: FAO, 17–25.
- Chen J Q, John R, Sun G, et al. 2018. Prospects for the sustainability of social-ecological systems (SES) on the Mongolian Plateau: five critical issues. *Environmental Research Letters*, 13(12): 123004, doi: 10.1088/1748-9326/aaf27b.
- Chen J Q. 2021. *Biophysical Models and Applications in Ecosystem Analysis*. East Lansing: Michigan State University Press, 89–118.
- Chen J Q, John R, Yuan J, et al. 2022. Sustainability challenges for the social-environmental systems across the Asian Drylands Belt. *Environmental Research Letters*, 17(2): 023001, doi: 10.1088/1748-9326/ac472f.
- Chen Z F, Wang W G, Fu J Y. 2020. Vegetation response to precipitation anomalies under different climatic and biogeographical conditions in China. *Scientific Reports*, 10(1): 830, doi: 10.1038/s41598-020-57910-1.
- Cong W W, Li X Y, Pan X B, et al. 2022. A new scientific framework of dryland ecological quality assessment based on IOAO principle. *Ecological Indicators*, 136: 108595, doi: 10.1016/j.ecolind.2022.108595.
- Coutts A M, Harris R J, Phan T, et al. 2016. Thermal infrared remote sensing of urban heat: Hotspots, vegetation, and an assessment of techniques for use in urban planning. *Remote Sensing of Environment*, 186: 637–651.
- Fan Y, Chen J Q, Shirkey G, et al. 2016. Applications of structural equation modeling (SEM) in ecological studies: an updated review. *Ecological Processes*, 5: 19, doi: 10.1186/s13717-016-0063-3.
- Fernandes T J G, del Campo A D, Herrera R, et al. 2016. Simultaneous assessment, through sap flow and stable isotopes, of water use efficiency (WUE) in thinned pines shows improvement in growth, tree-climate sensitivity and WUE, but not in WUEi. *Forest Ecology and Management*, 361: 298–308.
- Fick S E, Hijmans R J. 2017. WorldClim 2: new 1-km spatial resolution climate surfaces for global land areas. *International Journal of Climatology*, 37(12): 4302–4315.
- Guo B B, Zhang J, Meng X Y, et al. 2020. Long-term spatio-temporal precipitation variations in China with precipitation surface interpolated by ANUSPLIN. *Scientific Reports*, 10(1): 81, doi: 10.1038/s41598-019-57078-3.
- Hang X, Li Y C, Luo X C, et al. 2020. Assessing the ecological quality of Nanjing during its urbanization process by using satellite, meteorological, and socioeconomic data. *Journal of Meteorological Research*, 34(2): 280–293.
- Huang J, Chen J H, Zhang F M. 2021. Spatio-temporal evolution of climate-induced reduction risk for winter wheat in Anhui Province based on principal component analysis. *Chinese Journal of Applied Ecology*, 32(9): 3185–3194. (in Chinese)
- Hutchinson M F, Xu T. 2013. Anusplin version 4.4 user guide. [2022-03-30]. <http://fennerschool.anu.edu.au/files/anusplin44.pdf>.
- IPCC. 2019. *Climate Change and Land: an IPCC special report on climate change, desertification, land degradation, sustainable land management, food security, and greenhouse gas fluxes in terrestrial ecosystems*. In: *Climate Change and Land*. Shukla P R, Skea J, Calvo Buendia E, et al. Geneva: IPCC.
- Jiang F, Zhang Y Q, Li J Y, et al. 2021. Research on remote sensing ecological environmental assessment method optimized by regional scale. *Environmental Science and Pollution Research*, 28(48): 68174–68187.
- John R, Chen J Q, Ou-Yang Z T, et al. 2013. Vegetation response to extreme climate events on the Mongolian Plateau from 2000 to 2010. *Environmental Research Letters*, 8(3): 035033, doi: 10.1088/1748-9326/8/3/035033.
- John R, Chen J, Lu N, et al. 2009. Land cover/land use change in semi-arid Inner Mongolia: 1992–2004. *Environmental Research Letters*, 4(4): 045010, doi: 10.1088/1748-9326/4/4/045010.
- Liu S L, Wang T. 2010. Regionalization for aeolian desertification control and countermeasures in the Otindag Sandy Land Region, China. *Journal of Desert Research*, 30(5): 999–1005. (in Chinese)
- Lou J P, Wang X M, Cai D W. 2019. Spatial and temporal variation of wind erosion climatic erosivity and its response to ENSO in the Otindag Desert, China. *Atmosphere*, 10: 614, doi: 10.3390/atmos10100614.
- Lu C X, Zhao T Y, Shi X L, et al. 2018. Ecological restoration by afforestation may increase groundwater depth and create potentially large ecological and water opportunity costs in arid and semiarid China. *Journal of Cleaner Production*, 176: 1213–1222.
- Ma W Y, Wang X M, Zhou N, et al. 2017. Relative importance of climate factors and human activities in impacting vegetation dynamics during 2000–2015 in the Otindag Sandy Land, northern China. *Journal of Arid Land*, 9(4): 558–567.

- Mamat Z, Halik Ü, Keyimu M, et al. 2018. Variation of the floodplain forest ecosystem service value in the lower reaches of Tarim River, China. *Land Degradation & Development*, 29(1): 47–57.
- Masroor M, Sajjad H, Rehman S, et al. 2022. Analysing the relationship between drought and soil erosion using vegetation health index and RUSLE models in Godavari middle sub-basin, India. *Geoscience Frontiers*, 13(2): 101312, doi: 10.1016/j.gsf.2021.101312.
- Niu L N, Shao Q Q, Ning J, et al. 2023. The assessment of ecological restoration effects on Beijing-Tianjin Sandstorm Source Control Project area during 2000–2019. *Ecological Engineering*, 186: 106831, doi: 10.1016/j.ecoleng.2022.106831.
- Priyadarshi N, Chowdary V M, Srivastava Y K, et al. 2018. Reconstruction of time series MODIS EVI data using de-noising algorithms. *Geocarto International*, 33(10): 1095–1113.
- Qureshi S, Alavipanah S K, Konyushkova M, et al. 2020. A remotely sensed assessment of surface ecological change over the Gomishan Wetland, Iran. *Remote Sensing*, 12(18): 2989, doi: 10.3390/rs12182989.
- Shao W Y, Wang Q Z, Guan Q Y, et al. 2022. Distribution of soil available nutrients and their response to environmental factors based on path analysis model in arid and semi-arid area of northwest China. *Science of The Total Environment*, 827: 154254, doi: 10.1016/j.scitotenv.2022.154254.
- Shi L, Zhang Z J, Zhang C Y, et al. 2004. Effects of sand burial on survival, growth, gas exchange and biomass allocation of *Ulmus pumila* seedlings in the Hunshandak Sandland, China. *Annals of Botany*, 94(4): 553–560.
- Sun B, Wang Y, Li Z Y, et al. 2019. Estimating soil organic carbon density in the Otindag Sandy Land, Inner Mongolia, China, for modelling spatiotemporal variations and evaluating the influences of human activities. *CATENA*, 179: 85–97.
- Tang L P, Ke X L, Chen Y Y, et al. 2021. Which impacts more seriously on natural habitat loss and degradation? Cropland expansion or urban expansion? *Land Degradation & Development*, 32(2): 946–964.
- Tian Q J, Min X J. 1998. Advances in study on vegetation indices. *Advances in Earth Science*, 13(4): 327–333. (in Chinese)
- Toy T J, Osterkamp W R. 1995. The applicability of RUSLE to geomorphic studies. *Journal of Soil and Water Conservation*, 50(5): 498–503.
- Wang J, Ma J L, Xie F F, et al. 2020. Improvement of remote sensing ecological index in arid regions: Taking Ulan Buh Desert as an example. *Chinese Journal of Applied Ecology*, 31(11): 3795–3804. (in Chinese)
- Wang J, Liu D X, Ma J L, et al. 2021. Development of a large-scale remote sensing ecological index in arid areas and its application in the Aral Sea Basin. *Journal of Arid Land*, 13(1): 40–55.
- Wang X M, Lou J P, Ma W Y, et al. 2017. The impact of reclamation on aeolian desertification of four species in the Otindag Desert, China. *CATENA*, 157: 189–194.
- Wei W, Shi S N, Zhang X Y, et al. 2020. Regional-scale assessment of environmental vulnerability in an arid inland basin. *Ecological Indicators*, 109: 105792, doi: 10.1016/j.ecolind.2019.105792.
- Wen H, Chen J Q, Wang Z F. 2020. Disproportioned performances of protected areas in the Beijing-Tianjin-Hebei Region. *Sustainability*, 12(16), 6404, doi: 10.3390/su12166404.
- Wu R N, Cong W W, Li Y H, et al. 2019. The scientific conceptual framework for ecological quality of the dryland ecosystem: Concepts, indicators, monitoring and assessment. *Journal of Resources and Ecology*, 10(2): 196–201.
- Wu S P, Gao X, Lei J Q, et al. 2022. Ecological environment quality evaluation of the Sahel region in Africa based on remote sensing ecological index. *Journal of Arid Land*, 14(1): 14–33.
- Wu Z T, Wu J J, Liu J H, et al. 2013. Increasing terrestrial vegetation activity of ecological restoration program in the Beijing–Tianjin Sand Source Region of China. *Ecological Engineering*, 52: 37–50.
- Xu H Q. 2013. A remote sensing index for assessment of regional ecological changes. *China Environmental Science*, 33(5): 889–897. (in Chinese)
- Xu H Q, Wang M Y, Shi T T, et al. 2018. Prediction of ecological effects of potential population and impervious surface increases using a remote sensing based ecological index (RSEI). *Ecological Indicators*, 93: 730–740.
- Xu H Q, Wang Y F, Guan H D, et al. 2019. Detecting ecological changes with a remote sensing based ecological index (RSEI) produced time series and change vector analysis. *Remote Sensing*, 11(20): 2345, doi: 10.3390/rs11202345.
- Xu L L, Yu G M, Zhang W J, et al. 2020. Change features of time-series climate variables from 1962 to 2016 in Inner Mongolia, China. *Journal of Arid Land*, 12(1): 58–72.
- Yang X Y, Meng F, Fu P J, et al. 2022a. Time-frequency optimization of RSEI: A case study of Yangtze River Basin. *Ecological Indicators*, 141: 109080, doi: 10.1016/j.ecolind.2022.109080.
- Yang X Y, Meng F, Fu P J, et al. 2022b. Instability of remote sensing ecological index and its optimisation for time frequency and scale. *Ecological Informatics*, 72: 101870, doi: 10.1016/j.ecoinf.2022.101870.

- Yao K X, Halike A, Chen L M, et al. 2022. Spatiotemporal changes of eco-environmental quality based on remote sensing-based ecological index in the Hotan Oasis, Xinjiang. *Journal of Arid Land*, 14(3): 262–283.
- Ye X, Kuang H H. 2022. Evaluation of ecological quality in southeast Chongqing based on modified remote sensing ecological index. *Scientific Reports*, 12(1): 15694, doi: 10.1038/s41598-022-19851-9.
- Yuan Z H, Bao G, Yin S, et al. 2016. Vegetation changes in Otindag sand country during 2000–2014. *Acta Prataculturae Sinica*, 25(1): 33–46. (in Chinese)
- Zhang Q, Yang Z S, Hao X C, et al. 2019. Conversion features of evapotranspiration responding to climate warming in transitional climate regions in northern China. *Climate Dynamics*, 52(7): 3891–3903.
- Zhao X, Wang P, Yasir M, et al. 2022. Decision support system based on spatial and temporal pattern evolution of ecological environmental quality in the Yellow River Delta from 2000 to 2020. *Soft Computing*, 26(20): 11033–11044.
- Zhao X H, Zhang F M, Han D C, et al. 2021. Evapotranspiration changes and its attribution in semi-arid regions of Inner Mongolia. *Arid Zone Reseach*, 38(6): 1614–1623. (in Chinese)
- Zheng Z H, Wu Z F, Chen Y B, et al. 2022. Instability of remote sensing based ecological index (RSEI) and its improvement for time series analysis. *Science of The Total Environment*, 814: 152595, doi: 10.1016/j.scitotenv.2021.152595.
- Zhu D Y, Chen T, Wang Z W, et al. 2021. Detecting ecological spatial-temporal changes by Remote Sensing Ecological Index with local adaptability. *Journal of Environmental Management*, 299: 113655, doi: 10.1016/j.jenvman.2021.113655.
- Zhuang Q W, Shao Z F, Huang X, et al. 2021. Evolution of soil salinization under the background of landscape patterns in the irrigated northern slopes of Tianshan Mountains, Xinjiang, China. *CATENA*, 206: 105561, doi: 10.1016/j.catena.2021.105561.

Appendix

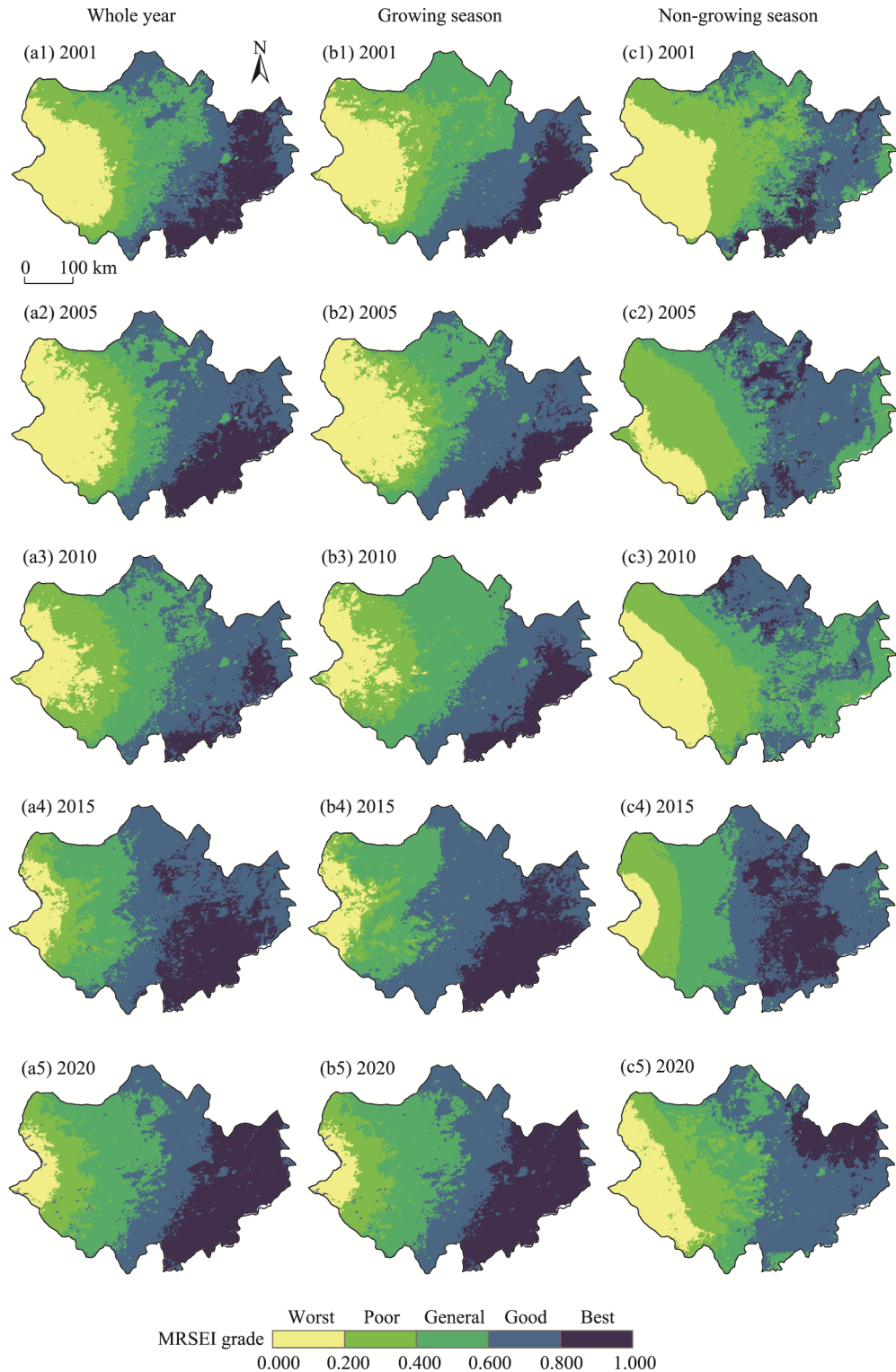


**Fig. S1** Spatial distributions of MRSEI at the whole year (a1–a5), growing season (b1–b5), and non-growing season (c1–c5) scales in 2001, 2005, 2010, 2015, and 2020 in Otindag Sandy Land